

# Invasion percolation of single component, multiphase fluids with lattice Boltzmann models

Michael C. Sukop\*, Dani Or

*Department of Civil & Environmental Engineering, University of Connecticut, Unit-2037, 261 Glenbrook Road, Storrs, CT 06269-2037, USA*

## Abstract

Application of the lattice Boltzmann method (LBM) to invasion percolation of single component multiphase fluids in porous media offers an opportunity for more realistic modeling of the configurations and dynamics of liquid/vapor and liquid/solid interfaces. The complex geometry of connected paths in standard invasion percolation models arises solely from the spatial arrangement of simple elements on a lattice. In reality, fluid interfaces and connectivity in porous media are naturally controlled by the details of the pore geometry, its dynamic interaction with the fluid, and the ambient fluid potential. The multiphase LBM approach admits realistic pore geometry derived from imaging techniques and incorporation of realistic hydrodynamics into invasion percolation models.

© 2003 Published by Elsevier B.V.

PACS: 47.55.Mh; 47.55.Kf; 92.40.Lg

Keywords: Lattice Boltzmann; Invasion percolation; Multiphase; Porous media

## 1. Introduction

Percolation models are capable of generating complex fluid invasion patterns similar to those observed in real inhomogeneous porous materials under certain conditions. The complex geometry of connected paths in such percolation models arises solely from the spatial arrangement of simple elements on a lattice. Typically, a network of channels is generated with channel sizes that vary randomly. In invasion percolation simulation

of drainage, non-wetting fluid advances by displacing wetting fluid and advancing into the channel adjacent to the invading front with lowest capillary resistance at each time step. The capillary pressure that must be overcome is given by the Young–Laplace equation:

$$P_{\text{cap}} = \frac{\gamma \cos \theta}{r}, \quad (1)$$

where  $\gamma$  is the interfacial tension between the fluids,  $\theta$  is the wetting angle, and  $r$  is channel radius. Because interfacial tension and wetting angle are considered constant,  $P_{\text{cap}}$  is inversely proportional to capillary radius. The channel to be invaded at each subsequent time step is simply the largest one available to the invading front.

\*Corresponding author. Currently at: Department of Earth Sciences, Florida International University, University Park, PC 344, 11200 SW 8th Street, Miami, FL 33199, USA. Fax: +1-305-348-3877.

E-mail address: [sukopm@fin.edu](mailto:sukopm@fin.edu) (M.C. Sukop).

Fluid properties and system boundary conditions can produce a wide range of displacement regimes in geometrically identical networks. Lenormand et al. [1] proposed a ‘phase diagram’ for the various patterns and flow regimes based on the interplay between the various forces characterized by capillary numbers and viscosity ratios (Fig. 1) that determines the nature of the displacement process when non-wetting fluid is injected into a medium saturated with wetting fluid (drainage). Gravitational effects can play an important role but are not considered here. The existence of such differences in the morphology of the invading front as a function of flow rate and fluid properties (surface tension, contact angle, and viscosity ratio), shows that invasion percolation based on network geometry alone is insufficient to capture the large variety of behaviors that can be observed in the same network. For an alternative approach that extends standard invasion percolation to include viscous effects, see Ref. [2].

Ideally, the lattice Boltzmann method (LBM) would be capable of simulating all three types of displacement shown on Fig. 1. In our current implementation, kinematic viscosity ( $\nu = \mu/\rho$ ) is equal in both the liquid and vapor phases; hence the viscosity ratio  $M$  is fixed at the density ratio of the vapor to liquid, i.e.,  $M = \rho_g/\rho_l$ , which is on the order of 0.1 in simulations presented here. We are

free to move vertically along the  $C_a$  axis (within limits) at  $\log M = -1$  but we cannot currently simulate viscous fingering. Invasion percolation simulates the capillary fingering domain, which is currently accessible to us. In future applications it should be possible to remove this viscosity limitation by relating  $\tau$  (the LBM relaxation time) to phase density (see Eq. (6)).

The primary advantage of the LBM over previous simulations (e.g., Refs. [1,3]) is its ability to incorporate fluid factors and complex details of pore shape that characterize realistic porous media in a physically sound way. Another feature of the method in the present study is that we consider a single component, multiphase system (e.g., water and its vapor). Numerous papers describing two component (e.g., oil/water) displacement simulations and processes in porous media have appeared. In contrast, little has been done with multiphase single component simulations. Several researchers [4,5] presented LB simulations of single component multiphase fluids in small model porous media using the ‘free-energy’ LB model of Swift et al. [6], which differs considerably from the model we use here. The Swift et al. model [6] has been criticized as being a ‘top down’ approach where macroscopic properties such as surface tension are prescribed [7]. In contrast, the Shan and Chen (SC) [8] model is a ‘bottom up’ approach

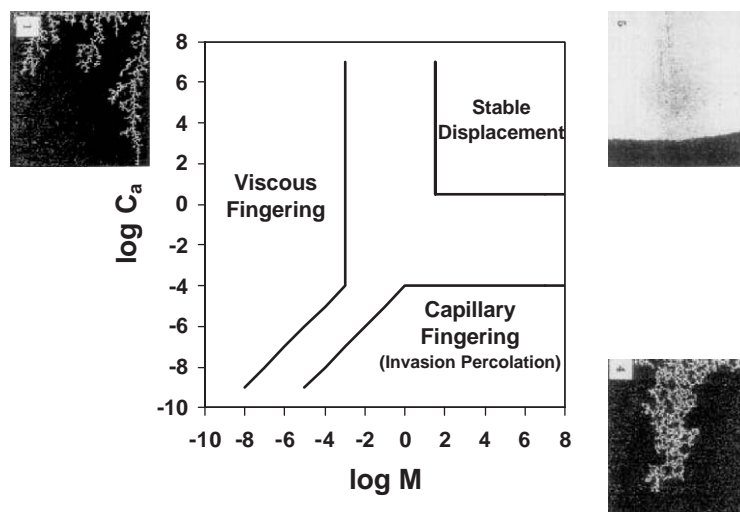


Fig. 1. Phase diagram of Lenormand et al. [1]. Reprinted with permission of Cambridge University Press.

where such macroscopic properties emerge from particle scale dynamics. Recent work by He and Doolen [9] suggests that elements of both the SC model (used in this paper) and the free energy model of Swift et al. [4] are necessary for a complete treatment of the relevant physics. Only two papers [10,11] appear to report on single component simulations involving solids carried out with the SC model. Neither of these investigates the potential for simulation of invasion percolation phenomena.

Our primary objective here is to demonstrate capabilities of the single component multiphase LBM for modeling interface advance in simple and more realistic pore networks based on first principles and without invoking interface routing algorithms [12]; interface movement arises naturally in the LBM and the effects of fluid properties, velocity, and geometrical details are naturally incorporated.

The paper is organized as follows: Section 2 provides information on the model and its configuration for addressing invasion percolation. Section 3 presents the results of simulations in network elements, while simulations in networks and natural porous media are given in Section 4. Conclusions are drawn in Section 5.

## 2. Methods

We use a two-dimensional, nine-velocity model (referred to as D2Q9) with single relaxation time. Details of this model are described elsewhere (e.g., Refs. [13,14]). Here, we briefly review some unique aspects of multiphase, single-component models. For simplicity, this is done with reference to the 7-velocity model on a triangular grid [8].

The principal distinguishing characteristic of multiphase, single-component models is the inclusion of a cohesive force between particles that leads to a non-ideal equation of state (EOS), which relates pressure and density:

$$P = \frac{c^2}{D} \left[ (1 - d_0)\rho + \frac{b}{D} G \psi^2(\rho) \right], \quad (2)$$

where  $c$  is the maximum particle speed in the model (1 lattice unit per time step [ $\text{lu ts}^{-1}$ ] for the

simplest 7-velocity model),  $D$  is the dimension of the model,  $d_0$  is the fraction of particles at rest,  $\rho$  is particle density (a function of space and time), and  $b$  is the number of velocity directions (6 on the 2D triangular grid and 8 on the square grid).  $G$  is an interaction strength that is negative for attraction between particles.

The function  $\psi$  can be varied arbitrarily to fit a given EOS but must be monotonic and bounded. It relates directly to the attractive force  $\mathbf{F}$  between nearest neighbor fluid particles:

$$\mathbf{F}(\mathbf{x}, t) = -G\psi(\mathbf{x}, t) \sum_{a=1}^6 \psi(\mathbf{x} + \mathbf{e}_a \Delta t, t) \mathbf{e}_a, \quad (3)$$

where  $\mathbf{e}_a$  is a unit velocity vector pointing in one of  $a = 1, 2, \dots, 6$  non-zero velocity directions on the triangular grid, and  $\Delta t$  is the model time step (ts); here  $\Delta t = 1$  ts.

A particular  $\psi$  function is given by [15]:

$$\psi(\rho) = \psi_0 \exp(-\rho_0/\rho). \quad (4)$$

This form of  $\psi$  leads to LB models whose “...behavior is consistent with that of an isothermal process...” with  $-(1 - d_0)/G$  as a temperature scale [15].  $\psi_0$  and  $\rho_0$  can be varied arbitrarily. All results here use this form of  $\psi$ . Fig. 2 shows Eq. (2) for a series of  $G$  values that result in behavior ranging from supercritical ( $G = 0$  and  $-3$ , no phase separation) to subcritical ( $G = -6$  and  $-7$ ). At subcritical  $G$ , two densities coexist at a single pressure and the fluid can separate into vapor and liquid phases.

For comparison, the water EOS is also presented in Fig. 2. Low compressibility of water relative to its vapor is indicated by the relative steepness of the curve in high and low density regions. In contrast, liquid compressibility in this LB EOS is greater than vapor phase compressibility.

### 2.1. Boundary conditions

Flow is induced with fixed velocity ( $\mathbf{u}_y = \text{constant}$ ,  $\mathbf{u}_x = 0$ ) boundary conditions at the vapor inlet and liquid outlet, in keeping with the typical experimental practice of constant flow rate. Implementation of constant velocity boundary conditions

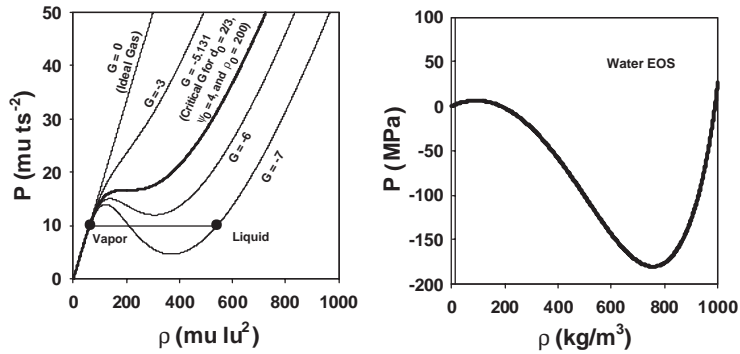


Fig. 2. Single-component, multiphase LBM non-ideal EOS for different values of  $G$  and EOS for water after Truskett et al. [16].  $lu$ ,  $mu$ , and  $ts$  refer to LBM lattice length units, mass units, and time step, respectively.

follows the approach proposed by Zou and He [17]. Periodic boundaries are applied in the  $y$  direction.

The initial density at the inlet and for several lattice units into the domain is set to the vapor density determined in solids-free simulations of a flat liquid–vapor interface. The initial liquid density in the rest of the active domain is determined the same way.

The internal walls use a simple bounce back boundary condition. They also exert an attractive force on the fluid via the method introduced by Martys and Chen [18]. The adhesive parameter is taken as a function of the cohesive force parameter so that for a particular equilibrium liquid density, the density of the adsorbed layer is approximately the same as the liquid. There has been discussion in the literature regarding breakdown of no-slip conditions imposed by bounce back boundary conditions during interface motion [4]. In our simulations of drainage, the adsorbed fluid layer may in a sense ‘lubricate’ the boundary and no obvious problems are observed.

### 2.2. Capillary number

The capillary number is computed using an approach similar to that suggested by Friedman [19], which uses average pore fluid velocity  $v = v_{in}/\theta_m$ , where  $v_{in}$  is the injected fluid velocity on the inlet boundary and  $\theta_m$  is areal liquid content.

Applying this approach and assuming a contact angle  $\theta = 0$ , the capillary number is

$$C_a = v_{in}\mu/\theta_m\gamma. \tag{5}$$

Calculation of  $C_a$  requires the surface tension  $\gamma$  of the liquid–vapor interface. We determine this empirically by fitting (1) to the observed pressure difference between the inside and outside of a series of vapor bubbles of varying radii (e.g., Ref. [15]). For the particular EOS we use, the 2D surface tension  $\gamma = 13.85\text{ lu mu ts}^{-2}$ , where  $mu$  refers to model mass units (1 ‘particle’ = 1  $mu$  here).

The viscosity of the D2Q9 LBM is [14]

$$\mu = \frac{c^2}{3} \left( \tau - \frac{\Delta t}{2} \right) \rho, \tag{6}$$

where  $\rho$  is an areal density ( $ML^{-2}$ ),  $\tau$  is the BGK relaxation time, and  $c$  is maximum speed on the lattice ( $1\text{ lu ts}^{-1}$ ).

For an invading vapor density of  $85.7\text{ mu lu}^{-2}$ , the viscosity is  $14.3\text{ mu ts}^{-1}$ , and the dimensionless capillary number is a function of the inlet velocity and fluid content only:  $C_a = 1.0v_{in}/\theta_m$ , with the units of  $v$  as  $\text{lu ts}^{-1}$ .

### 3. Simulations in network elements

Simulation of interface movement and the ability of the invading fluid to discriminate between pores of different size are crucial to simulation of larger networks. In this section, we demonstrate the invading fluid’s selectivity for the largest available pore and show how this is affected by  $C_a$ .

Fig. 3 shows invasion of injected vapor phase through a perforated plate with holes of varying

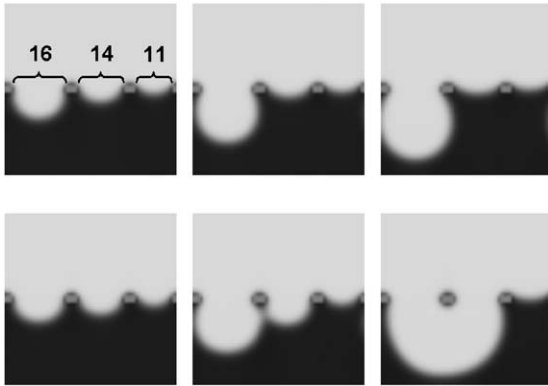


Fig. 3. Invasion of vapor through plate with perforations of 16, 14 and 11  $\mu\text{m}$  at  $C_a = 10^{-3}$  (top) and  $C_a = 10^{-2}$  (bottom). Gray scale proportional to density.

size at two different  $C_a$ . In the upper time sequence of images at low  $C_a$ , only the largest pore is invaded. In contrast, the bottom sequence shows invasion of the 2 largest pores at larger  $C_a$  when viscous effects become more important. These results are similar to those obtained in Ref. [5] with the free energy model. Selectivity for the largest pore was demonstrated but the effect of  $C_a$  was not investigated.

#### 4. Simulations in networks

Our network simulations are rudimentary due to computational constraints but appear to be quite realistic in their treatment of fluid physics. First, we show simulations in random networks of pores generated by sparse distributions of disks and squares at different  $C_a$ . Finally, we show results for a realistic natural porous medium.

##### 4.1. Capillary number and geometry effects

Fig. 4 illustrates the effects of changes in  $C_a$  and details of geometry. Each simulation is carried out on a  $200 \times 200$  lattice with the same random arrangement of either squares or disks of three different sizes. For the disks,  $r = 2.5, 3.5$ , or  $4.5 \mu\text{m}$ , and squares occupying the same positions have side length  $2r$ . Results near breakthrough for two  $C_a$  are shown. The domains are periodic in the  $x$

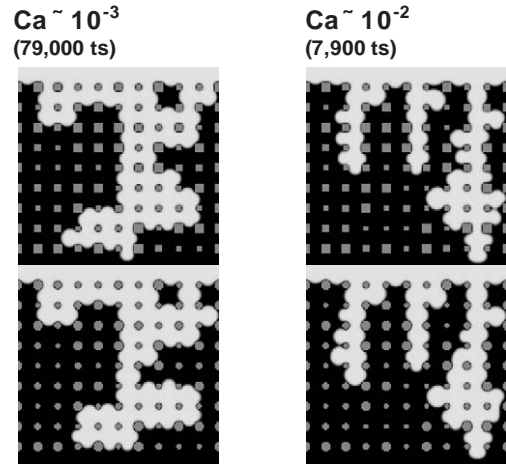


Fig. 4. Invasion into model porous media composed of randomly sized squares (top) and disks (bottom) at 2 capillary numbers.

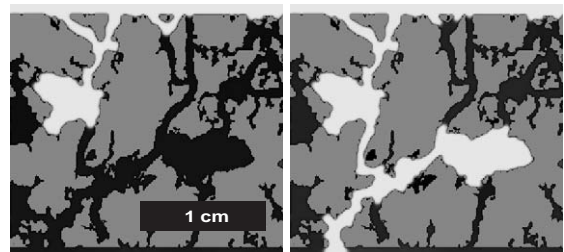


Fig. 5. Drainage in a cross-section of a real soil at 500,000 (left) and 1 million ts (right).  $C_a = 10^{-4}$ .

direction, although disks and squares at the left and right edges of the domain are fixed at large size and effectively bound the invasion process. The invasion patterns are more linear at higher  $C_a$ . There are also subtle differences in the invasion patterns for the two geometries at identical  $C_a$ . Such differences might be difficult to generate in a simplified bond network typical of invasion percolation simulations.

##### 4.2. Drainage in a real soil

Fig. 5 shows drainage (invasion of vapor phase) in a cross-section of real soil [20]. The original digitized image of the soil was modified to enhance connectivity, which is often too low in 2D sections of soils to allow percolation. Snap-shots of the

drainage process are shown at 0.5 million and 1 million time steps. The sequence of events during drainage is much richer than can be depicted in these snap-shots and we have placed a movie at <http://www.engr.uconn.edu/enviro/ephysics/research/00005d.gif>.

## 5. Conclusions

Lattice Boltzmann simulations in simplified network elements and small networks illustrate the viability of the method for computing invasion percolation phenomena in geometrically complex porous media. The LBM has the advantage of handling  $C_a$  higher than those representative of quasistatic drainage, which is typically invoked in invasion percolation. Fluid factors, represented by dimensionless  $C_a$  and viscosity ratio (when gravitational influences can be neglected), play important roles in displacement processes and are generally not considered in standard invasion percolation. We demonstrate the impact of changes in  $C_a$  and in the details of solid obstacle shapes.

## References

- [1] R. Lenormand, et al., *J. Fluid Mech.* 189 (1988) 165.
- [2] R.J. Glass, et al., *Water Resour. Res.* 37 (2001) 1197.
- [3] E. Aker, et al., *Transp. Porous Media* 32 (1998) 163.
- [4] A.J. Briant, et al., *Philos. Trans. Roy. Soc. London* 360 (2002) 485.
- [5] A.D. Angelopoulos, et al., *Phys. Rev. E* 57 (1998) 3237.
- [6] M.R. Swift, et al., *Phys. Rev. E* 54 (1996) 5041.
- [7] J. Chin, et al., *Philos. Trans. Roy. Soc. London* 360 (2002) 547.
- [8] X. Shan, H. Chen, *Phys. Rev. E* 47 (1993) 1815.
- [9] X. He, G.D. Doolen, *J. Stat. Phys.* 107 (2002) 309.
- [10] P. Raïskinmäki, et al., *J. Stat. Phys.* 107 (2002) 143.
- [11] P. Raïskinmäki, et al., *Comput. Mat. Sci.* 18 (2000) 7.
- [12] M.J. Blunt, H. Scher, *Phys. Rev. E* 52 (1995) 6387.
- [13] S. Succi, *The Lattice Boltzmann Equation for Fluid Dynamics and Beyond*, Clarendon Press, Oxford, 2001, 288pp.
- [14] D.A. Wolf-Gladrow, *Lattice-Gas Cellular Automata and Lattice Boltzmann Models: An Introduction*, Springer, Berlin, 2000, 308pp.
- [15] X. Shan, H. Chen, *Phys. Rev. E* 49 (1994) 2941.
- [16] T.M. Truskett, et al., *J. Chem. Phys.* 111 (1999) 2647.
- [17] Q. Zou, X. He, *Phys. Fluids* 9 (1997) 1591.
- [18] N.S. Martys, H. Chen, *Phys. Rev. E* 53 (1996) 743.
- [19] S.P. Friedman, *J. Adhes. Sci. Technol.* 13 (1999) 1495.
- [20] A.J. Ringrose-Voase, *J. Soil Sci.* 38 (1987) 343.